Model Predictive Control-Based Virtual Inertia Emulator for an Islanded Alternating Current Microgrid

Zheng, Changming; Dragicevic, Tomislav; Blaabjerg, Frede

Published in:
I E E E Transactions on Industrial Electronics

DOI (link to publication from Publisher):
10.1109/TIE.2020.3007105

Publication date:
2021

Document Version
Accepted author manuscript, peer reviewed version

Model Predictive Control Based Virtual Inertia Emulator for an Islanded AC Microgrid

Changming Zheng, *Student Member, IEEE*, Tomislav Dragičević, *Senior Member, IEEE*, and Frede Blaabjerg, *Fellow, IEEE*

***Abstract*—Conventional primary control employs outer-loop droop and inner-loop cascaded linear control to realize local voltage regulation and power-sharing of an islanded ac microgrid. However, it has a complex structure, limited dynamic response and a rapid rate of change of frequency when disturbances occur. This paper resolves these issues by proposing a model predictive control based virtual synchronous generator (VSG-MPC). An improved finite-set MPC is first proposed for the inner loop, achieving simplified control structure, faster dynamic response, enhanced bandwidth and stability, as well as improved current limitation. In the outer control loop, a simplified VSG without a phase-locked loop is employed to realize active power-sharing and inertia emulation. The merits above are verified by a description function of MPC and the frequency-domain response of the overall VSG. Simulation and experimental results verify the feasibility of the proposed method.**

***Index Terms*—Predictive control, voltage source converter, virtual synchronous generator (VSG), microgrid.**

I. Introduction

ALTERNATING current (ac) microgrid (MG) plays an increasingly significant role in the realization of high penetration of distributed energy resources (DERs), which can either be configured in grid-connected mode or islanded mode [1], [2]. In an ac MG, voltage source converters (VSCs) act as key interfaces between DERs and a common ac bus. Since an ac MG can manipulate multiple VSCs, it operates in a more flexible fashion than an individual DER unit. Nonetheless, control of VSC-based ac MG is still challenging since it inherently lacks a stiff voltage source and inertia. Generally, VSCs for ac MGs can be classified as grid-forming, grid-feeding, and grid-supporting converters by their functionality. Thereof, the former ones are crucial elements for islanded (stand-alone) operation of ac MGs, which aims to provide voltage and frequency support.

Hence, exploring an effective control scheme for VSCs is vital to guarantee reliable operation of an islanded ac MG. A typical control scheme comprises a three-level hierarchical control framework, i.e., primary, secondary, and tertiary control levels [3]–[5]. This paper focuses on optimizing the primary control, which comprises two main control loops, i.e., inner loop for local voltage and frequency regulation, and outer loop for power-sharing. The inner control loop is fundamental for stabilizing the whole system, where the DERs are controlled as grid-forming VSCs. The control objectives are to achieve desired static and dynamic voltage tracking performance (e.g., to meet the requirement of the IEC62040 standard for uninterrupted power supply applications). Conventionally, a cascaded dual-loop linear feedback control (i.e., voltage and current control loops with a modulator) is deployed in the inner loop of primary control. However, this control scheme suffers from a complex structure, slow transient response, limited control bandwidth, and tedious parameter-tuning effort [6]. Moreover, it is hard for a linear controller to handle the multi-objective optimization and various system constraints [7]–[9].

On the other hand, for the outer loop of primary control, droop control with a virtual impedance loop is usually employed to achieve accurate power-sharing and plug and play capability. With the increasing penetration of the inertia-less DERs in islanded ac MGs, conventional droop control scheme cannot provide enough inertia, thus leading to a rapid rate of change of frequency (ROCOF) when disturbances occur. Consequently, fluctuations in DERs or loads may considerably influence the system power-frequency stability. In this context, a virtual synchronous generator (VSG) concept is proposed [10]–[16], which aims to emulate the inertia of synchronous generators (SGs). Essentially, VSG can be equivalent to a modified droop control with a dedicated first-order lead-lag unit [10], [11]. Nevertheless, VSG still has a more intuitive physical meaning and a more direct implementation for inertia emulation. Various VSG schemes to date have been proposed, which can be grouped into current-controlled or voltage-controlled VSGs. In [12], [13], a current-controlled VSG scheme is first proposed. However, this method only deploys a current control loop, which cannot operate in an islanded mode. In [11], [14], a voltage-controlled VSG scheme is proposed, which supports the islanded-mode operation. However, it only deploys a single voltage control loop, thus lacking the current-limiting capability. Further, a cascaded linear control based VSG scheme is proposed in [15]–[17], which enables both voltage and current control. Nevertheless, this method still inherits the drawbacks of conventional linear control.

Model predictive control (MPC), especially finite-set MPC (FS-MPC), has proved to have a simple structure, inherent fast dynamic response, flexible multi-objective optimization and constraint-handling ability compared to linear control [6]–[9].

Manuscript received Month xx, 2019; revised Month xx, xxxx; accepted Month x, 2020. (*Corresponding author: Changming Zheng.*)

C. Zheng is with the College of Control Science and Engineering, China University of Petroleum (East China), Qingdao, 266580, China (e-mail: jsxzzcm@126.com).

T. Dragičević is with the Center of Electric Power and Energy, Technical University of Denmark, 2800 Kgs. Lyngby, Denmark (e-mail: tomdr@elektro.dtu.dk).

F. Blaabjerg is with the Department of Energy Technology, Aalborg University, Aalborg 9220, Denmark (e-mail: fbl@et.aau.dk).

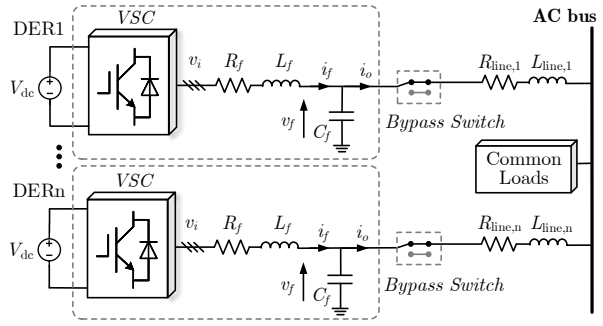

Fig. 1. Topology of a VSC-based islanded ac MG.

Generally, FS-MPC integrates multiple control objectives and constraints into a single cost function (CF). As a result, the cascaded structure and complex parameter-tuning process in conventional linear control schemes are avoided. Moreover, FS-MPC directly manipulates the optimal switching states without using a modulator, which reduces the implementation complexity and generates a fast dynamic response. Hence, FS-MPC manifests great potential for control of VSCs in ac MGs. Recently, applying FS-MPC scheme to ac MGs has attracted an increasing attention [6], [9]. In [6], a droop control based FS-MPC scheme is proposed for the fast and robust operation of an ac MG. However, the theoretical analysis is insufficient and experimental evaluation for paralleled-VSC operation is not provided. Also, a large ROCOF would be caused. In [9], an FS-MPC scheme is incorporated into VSG, which aims solely to improve the fault ride-through capability for MGs. However, since the cross-coupling effect between the state variables (i.e., inductor current and capacitor voltage) are not fully considered, optimal steady-state voltage and power-sharing performance cannot be guaranteed [18].

Motivated by the problems above, this paper proposes a VSG-MPC scheme for islanded ac MGs to optimize conventional primary control. Our contributions are as follows:

1) The proposed scheme combines an improved FS-MPC with a voltage-controlled VSG, achieving a compact structure, enhanced transient response and robustness of local voltage, as well as inertia emulation for islanded ac MGs.

2) The description function of FS-MPC and the frequency-domain response of proposed VSG-MPC are compared with linear-control based VSG, verifying that faster dynamic response, higher bandwidth of FS-MPC, as well as enhanced system stability can be obtained by the proposed method.

3) Enhanced current-limiting capability and robustness to model mismatches are achieved by the proposed VSG-MPC.

The rest of this work is arranged below. The modeling of the system is described in Section II. Section III introduces the conventional primary control of an ac MG. Section IV elaborates the principle of the proposed VSG-MPC scheme. Section V provides the simulation and experimental results, and Section VI concludes the work.

II. Modeling of The System

Fig. 1 depicts an islanded ac microgird fed by paralleled two-level three phase VSCs with output *LC* filters. The block

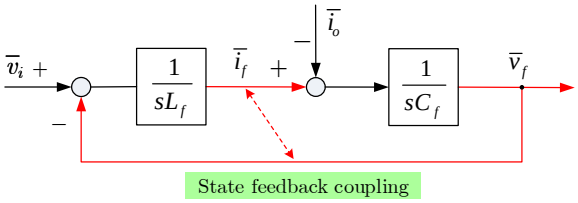

Fig. 2. Block diagram of an *s*-domain LC filter model.

TABLE I
Switching States and Voltage Vectors of a VSC

Index n	Switching state S_n			Voltage vector $\bar{v}_{i,n}$	
	$S_{a,n}$	$S_{b,n}$	$S_{c,n}$	$v_{i\alpha,n}$	$v_{i\beta,n}$
0	{0	0	0}	0	0
1	{1	0	0}	$2V_{dc}/3$	0
2	{1	1	0}	$V_{dc}/3$	$\sqrt{3}V_{dc}/3$
3	{0	1	0}	$-V_{dc}/3$	$\sqrt{3}V_{dc}/3$
4	{0	1	1}	$-2V_{dc}/3$	0
5	{0	0	1}	$-V_{dc}/3$	$-\sqrt{3}V_{dc}/3$
6	{1	0	1}	$V_{dc}/3$	$-\sqrt{3}V_{dc}/3$
7	{1	1	1}	0	0

diagram of an LC filter model in *s*-domain is depicted in Fig. 2. Based on Fig. 2, the continuous-time system dynamic model can be constructed as

$$\underbrace{\frac{d}{dt}\begin{bmatrix}\bar{i}_f\\ \bar{v}_f\end{bmatrix}}_{\dot{\mathbf{x}}(t)} = \underbrace{\begin{bmatrix}0 & -\frac{1}{L_f}\\ \frac{1}{C_f} & 0\end{bmatrix}}_{\mathbf{A}}\underbrace{\begin{bmatrix}\bar{i}_f\\ \bar{v}_f\end{bmatrix}}_{\mathbf{x}(t)} + \underbrace{\begin{bmatrix}\frac{1}{L_f} & 0\\ 0 & -\frac{1}{C_f}\end{bmatrix}}_{\mathbf{B}}\underbrace{\begin{bmatrix}\bar{v}_i\\ \bar{i}_o\end{bmatrix}}_{\mathbf{u}(t)} \tag{1}$$

where L_f and C_f are filter inductance and capacitance. The filter-capacitor voltage $\bar{v}_f = v_{f\alpha} + jv_{f\beta}$, filter-inductor current $\bar{i}_f = i_{f\alpha} + ji_{f\beta}$, converter output voltage $\bar{v}_i = v_{i\alpha} + jv_{i\beta}$ (total eight voltage vectors are determined by eight switching states, which are shown in Table I), and the load current $\bar{i}_o = i_{o\alpha} + ji_{o\beta}$ are defined in a stationary α-β frame using an amplitude-invariant Clarke transformation.

It should be noted that there exists a cross-coupling effect between the system state variables: inductor current and capacitor voltage, which would significantly degrade the system performance if it is not tackled correctly [18].

III. Conventional Primary Control of AC MG

Fig. 3 depicts a conventional primary control scheme for an islanded ac MG. As is shown, conventional primary control contains two main control loops, i.e., outer-loop droop control and inner-loop cascaded voltage and current control.

A. Outer-Loop Droop Control

The outer control loop is responsible for accurate power sharing of DERs and reference voltage and frequency generation for inner control loop. Typically, a P/Q droop control is described as [3]

$$\begin{cases}\omega_{\text{ref}} = \omega_n - k_p\left(P_{out} - P_{\text{ref}}\right)\\ V_{\text{ref}} = V_n - k_q\left(Q_{out} - Q_{\text{ref}}\right)\end{cases} \tag{2}$$

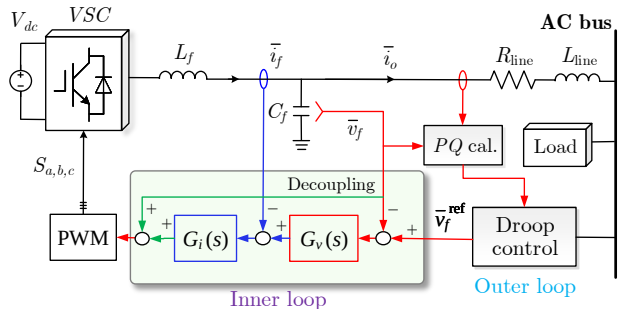

Fig. 3. Conventional primary control of an ac MG.

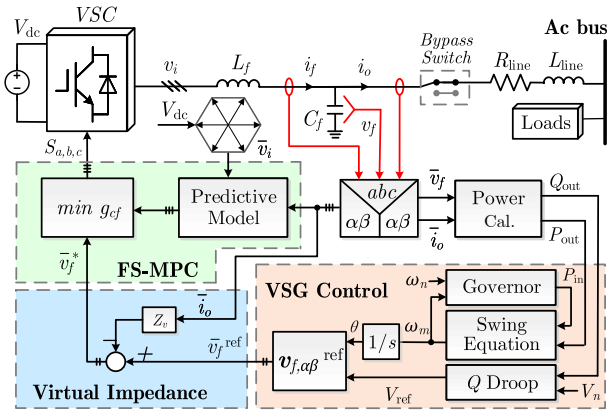

Fig. 4. Block diagram of proposed VSG-MPC scheme.

where ω_{ref}, V_{ref} and P_{ref} are reference angular frequency, voltage amplitude and active power, $\omega_n = 2\pi f_n$ and V_n are nominal angular frequency and voltage amplitude, k_p and k_q are $P-\omega$ and $Q-V$ droop coefficients, and P_{out} and Q_{out} are instantaneous active and reactive powers.

B. Inner-Loop Cascaded Linear Control

For an islanded ac MG, the DERs are normally controlled as voltage-controlled grid-forming VSCs to regulate the output voltage. Hence, the inner control loop aims to obtain desired voltage tracking response. Normally, a cascaded linear voltage and current controller is deployed, i.e., inner-loop proportional current controller $G_i(s)$ and outer-loop proportional-resonance (PR) voltage controller $G_v(s)$ as follows

$$G_i(s) = k_{pi} = 2\pi f_{bw} L_f \tag{3}$$

$$G_v(s) = k_{pv} + k_{rv}\frac{s}{s^2+\omega_n^2} \tag{4}$$

where k_{pi} and f_{bw} are proportional gain and desired bandwidth of the current controller, k_{pv} and k_{rv} are proportional and resonant gains of the voltage controller, and w_n is the fundamental angular frequency.

To address the drawbacks of conventional droop and cascaded linear control, a new MPC-based VSG (VSG-MPC) scheme is proposed.

IV. Proposed VSG-MPC Scheme for ac MGs

The proposed VSG-MPC control scheme mainly contains two parts, which are depicted in Fig. 4. In the inner loop, an improved FS-MPC with a virtual impedance loop is proposed to achieve the desired dynamic response and robustness of local voltage. In the outer loop, a simplified voltage-controlled VSG scheme is deployed to obtain accurate power-sharing as well as inertia emulation for an islanded ac MG, which is elaborated below.

A. Improved FS-MPC Based Voltage Control

An improved FS-MPC is proposed to obtain a higher bandwidth, faster dynamic response and enhanced robustness of output voltage compared to cascaded linear control.

1) Predictive Model Formulation: Based on the system dynamics (1), utilizing a zero-order-hold strategy, the state-space-averaging based predictive mode is formulated as

$$\underbrace{\begin{bmatrix}\bar{i}^p_{f,k+1}\\ \bar{v}^p_{f,k+1}\end{bmatrix}}_{\mathbf{x}^p_{k+1}} = \underbrace{\begin{bmatrix}\Phi_{11} & \Phi_{12}\\ \Phi_{21} & \Phi_{22}\end{bmatrix}}_{\mathbf{\Phi}}\underbrace{\begin{bmatrix}\bar{i}_{f,k}\\ \bar{v}_{f,k}\end{bmatrix}}_{\mathbf{x}_k} + \underbrace{\begin{bmatrix}\Gamma_{11} & \Gamma_{12}\\ \Gamma_{21} & \Gamma_{22}\end{bmatrix}}_{\mathbf{\Gamma}}\underbrace{\begin{bmatrix}\bar{v}_{i,k}\\ \bar{i}_{o,k}\end{bmatrix}}_{\mathbf{u}_k} \tag{5}$$

where $\mathbf{\Phi} = e^{\mathbf{A}T_s}$ and $\mathbf{\Gamma} = \int_0^{T_s} e^{\mathbf{A}\tau}\mathbf{B}d\tau$, and T_s is the sampling period.

2) Control Delay Compensation: In digital implementations, to compensate an inherent computational delay, a two-step forward prediction approach is employed, which is implemented by predicting the $k+2$ instant values of inductor current and capacitor voltage using (5)

$$\bar{i}^p_{f,k+2} = \Phi_{11}\bar{i}^p_{f,k+1} + \Phi_{12}\bar{v}^p_{f,k+1} + \Gamma_{11}\bar{v}_{i,k+1} + \Gamma_{12}\bar{i}_{o,k+1} \tag{6}$$

$$\bar{v}^p_{f,k+2} = \Phi_{21}\bar{i}^p_{f,k+1} + \Phi_{22}\bar{v}^p_{f,k+1} + \Gamma_{21}\bar{v}_{i,k+1} + \Gamma_{22}\bar{i}_{o,k+1} \tag{7}$$

where $\bar{i}_{o,k+1}$ can be directly substituted with $\bar{i}_{o,k}$ since the dynamics of the load current is very slow [8].

3) Dual-objective CF Design: Conventional FS-MPC in [19] only considers the single-voltage control objective, which neglects the coupling effect of the LC filter and may not achieve optimal steady-state voltage control performance [18]. Hence, to enhance output voltage control accuracy, both capacitor voltage and inductor current tracking objectives are integrated into the proposed CF as

$$g_{cf} = \left\|\bar{v}^*_f - \bar{v}^p_{f,k+2}\right\|^2 + \lambda\left\|\bar{i}^*_f - \bar{i}^p_{f,k+2}\right\|^2 + I_{\text{lim}} \tag{8}$$

where $\bar{v}^p_{f,k+2}$ and $\bar{i}^p_{f,k+2}$ are obtained by (6) and (7), λ is a weighting factor, and the capacitor voltage reference is

$$\bar{v}^*_f = V_{\text{ref}}\cos(\omega_{\text{ref},k}) + jV_{\text{ref}}\sin(\omega_{\text{ref},k}) \tag{9}$$

where V_{ref} and ω_{ref} are reference voltage magnitude and angular frequency, respectively.

Since the desired voltage steady-state equilibrium point is that the feedback capacitor voltage equals to its reference in (1), by replacing $\bar{v}_f$ with $\bar{v}^*_f$, the inductor current reference can be derived as

$$\bar{i}^*_f = jC_f\omega_{\text{ref},k}\bar{v}^*_f + \bar{i}_{o,k}. \tag{10}$$

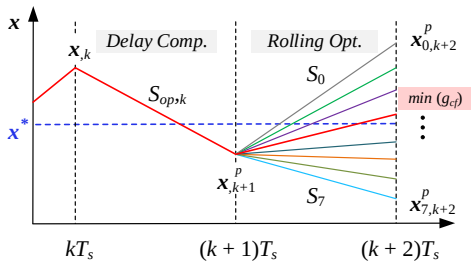

Fig. 5. Operating principle of rolling optimization in proposed FS-MPC.

It should be mentioned that the load current is explicitly included in (10), which essentially integrates the feed-forward compensation of the load-current disturbance. As a result, the voltage robustness against the load disturbance is significantly enhanced. Further, since FS-MPC allows multiple control objectives in the CF, $I_{\rm lim}$ in (8) is a secondary control objective term to limit the inductor current for over-current protection, which is expressed as

$$I_{\rm lim} = \begin{cases} \infty, & \text{if } \|\bar{i}_{f,k+2}\| > I_{\max} \\ 0, & \text{if } \|\bar{i}_{f,k+2}\| \le I_{\max} \end{cases} \tag{11}$$

where $I_{\max}$ is the maximum allowable inductor current limit.

4) Rolling Optimization: The operating principle of the rolling-optimization of the proposed FS-MPC is depicted in Fig. 5. As is shown, the delay compensation is first performed. Then, by substituting all candidate voltage vectors into the CF in (8), the optimal voltage vector that minimizes g_{cf} is chosen (see red line in Fig. 5) and applied to the VSCs.

Note that the proposed FS-MPC (with only one design parameter λ) eliminates the cascaded structure and modulation delay in conventional linear control schemes (with at least three design parameters in (3) and (4)), thus simplifying the control complexity, parameter tuning, and enhancing the system dynamic response. Moreover, once the future inductor current tends to exceed I_{max} in (11), corresponding voltage vectors would be directly discarded and strict current-limiting capability can be guaranteed.

B. Voltage-Controlled VSG For Inertia Emulation

To realize the accurate active power-sharing and to provide the inertia support for islanded ac MGs, a simplified voltage-controlled VSG scheme is employed to replace the conventional droop control, which also provides the voltage reference for inner control loops [20]. The block diagram of a simplified VSG is shown in Fig. 6, which contains three basic parts below.

1) Governor: The governor aims to adjust the active power in the case of frequency deviation, which is implemented by $\omega - P$ droop control

$$P_{in} = P_n - k_\omega(\omega_m - \omega_n) \tag{12}$$

where P_{in} and ω_m are virtual active power reference and virtual angular frequency of VSG. P_n and $\omega_n = 2\pi f_n$ are nominal active power and nominal angular frequency. $k_\omega = 1/k_p$ is the $\omega - P$ droop coefficient.

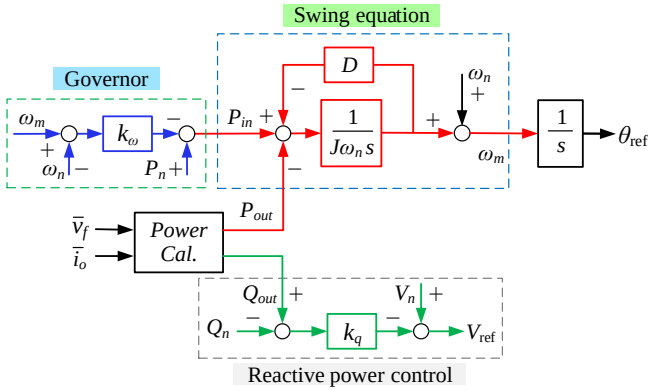

Fig. 6. Block diagram of simplified voltage-controlled VSG scheme.

2) Swing Equation for Inertia Emulation: To emulate the rotor inertia of SGs, a simplified swing equation is incorporated into the VSG control part as

$$P_{in} - P_{out} - D(\omega_m - \omega_n) \approx J\omega_n \frac{d(\omega_m - \omega_n)}{dt} \tag{13}$$

$$P_{out} = (v_{f\alpha} i_{o\alpha} + v_{f\beta} i_{o\beta}) \frac{\omega_c}{s + \omega_c} \tag{14}$$

where P_{out}, ω_c, D and J are output active power of VSC, cut-off frequency a low-pass filter, damping factor and moment of virtual inertia, respectively. For simplicity, the number of pole pairs of the VSG is assumed to be 1.

It should be mentioned that (13) is a simplified version of typical VSG by replacing the ac-bus frequency with the nominal ω_n, avoiding using the phase-locked loop [16]. Then, the damping factor D in (13) is equivalent to the droop coefficient k_ω in (12), which means either D or the governor can be omitted [11], [20]. Moreover, by introducing the feedforward of ω_n before ω_m, the rotor starting time is eliminated without affecting the steady-state response. When the frequency deviations exist, J is enabled to attenuate the ROCOF, thereby enhancing the power-frequency stability.

3) Reactive Power Control: Regarding the reactive power control, a $Q - V$ droop control is usually adopted by

$$V_{\rm ref} = V_n - k_q(Q_{out} - Q_n) \tag{15}$$

$$Q_{out} = (v_{f\beta} i_{o\alpha} - v_{f\alpha} i_{o\beta}) \frac{\omega_c}{s + \omega_c} \tag{16}$$

where $V_{\rm ref}$, $V_{\rm n}$, Q_{out} and Q_n are voltage reference amplitude for inner loop, nominal voltage amplitude, reactive power and nominal reactive power. k_q is the $Q - V$ droop coefficient.

Finally, the reference voltage amplitude $V_{\rm ref}$ in (15) and the angular frequency ω_m in (13) will synthesize the voltage reference $\bar{v}_f^{\rm ref}$ for inner control loops as shown in Fig. 4.

C. Virtual Impedance Loop

Note that different line impedance may affect the power sharing accuracy. To mitigate this adverse effect, a virtual impedance is normally utilized to shape the output impedance without losing efficiency. Hence, the inner-loop voltage reference with a virtual-impedance loop is modified as

$$\bar{v}_f^* = \bar{v}_f^{\rm ref} - Z_v \bar{i}_o \tag{17}$$

TABLE II
COMPARISON BETWEEN PROPOSED VSG-MPC AND PRIOR PRIMARY CONTROL SCHEMES FOR ISLANDED AC MGS

Comparative item	Droop-Linear control [3]	VSG-Linear control [17]	Proposed VSG-MPC
Block diagram	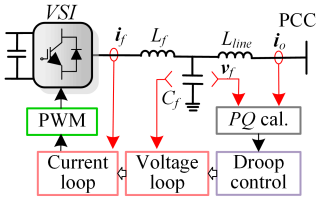	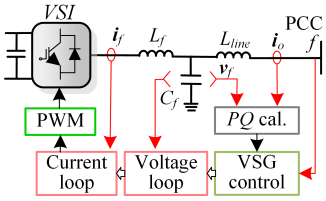	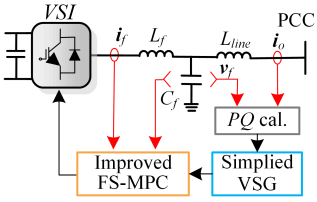
Control-loop number	Three	Three	Two
Inertia emulation	Requires dedicated unit	Yes	Yes
Modulation stage	PWM or SVM	PWM or SVM	Not required
Multi-objective optim.	Cannot be solved	Cannot be solved	Easy to solve
Parameter-tuning effort	Complex	Complex	Very simple
Steady-state response	Good	Good	Good
Dynamic performance	Moderate	Moderate	Very fast
Current-limiting capacity	Unavoidable over-current ripple	Unavoidable over-current ripple	Strict current limit

where $\bar{v}_f^* = \bar{v}_{f\alpha}^* + j\bar{v}_{f\beta}^*$ is the final voltage reference fed to the inner FS-MPC loop in (9). $Z_v = R_v + j\omega L_v$ is the preset virtual impedance, and R_v aims to damp the synchronous resonance [21].

D. Comparison with Prior Primary Control Schemes

The proposed VSG-MPC scheme is comprehensively compared with prior primary control schemes for an islanded ac MG in Table II. First, conventional Droop-Linear control cannot provide enough inertia. Although a modified droop control can be equivalent to VSG by adding a dedicated lead-lag unit, it is still not as intuitive as the direct implementation of VSG [11]. Second, the proposed FS-MPC (single loop with only one design parameter) eliminates the cascaded structure in conventional linear control schemes (dual loops with at least three design parameters), thus simplifying the implementation complexity and parameter-tuning efforts. Also, the proposed VSG-MPC does not need to measure the ac-bus frequency as in [17], which avoids the phase-locked loop. Meanwhile, the proposed VSG-MPC does not require a modulator like conventional linear-control based schemes, resulting in a reduced computational delay and inherent faster dynamic performance. Another attractive merit of the proposed VSG-MPC is that it can simply tackle the multi-objective optimization (such as harmonic spectrum shaping and switching frequency regulation), which is hard to solve by conventional Droop-Linear or VSG-Linear control. Moreover, the proposed VSG-MPC can obtain a strict current-limiting capability while conventional linear-control based schemes have unavoidable over-current ripple. This is due to the differences between FS-MPC and conventional linear control in constraint-handling principle, which will be elaborated in Section V-*D* later.

E. Frequency-Domain Stability Analysis

Since inner-loop FS-MPC is essentially a nonlinear control method, of which stability analysis is still an open issue [9].

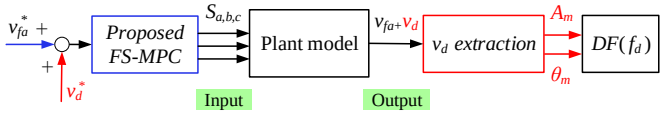

Fig. 7. Basic principle of DF extraction for proposed FS-MPC.

To solve this issue, a describing function (DF) method is employed in this paper to first derive the closed-loop frequency-domain model of the proposed FS-MPC. The basic principle is depicted in Fig. 7. To be specific, an ac-voltage-perturbation frequency sweep is conducted using numerical simulations. By applying a small sinusoidal voltage perturbation v_d^* to the inner-loop phase-voltage reference v_{fa}^* with an amplitude $A_d = 50$ V and a frequency f_d varying from 100 Hz to 5 kHz, the closed-loop DF of proposed FS-MPC is obtained by

$$DF(f_d) = \frac{A_m(f_d)}{A_d} \angle\theta_m(f_d) \tag{18}$$

where $A_m(f_d)$ and $\angle\theta_m(f_d)$ are the extracted output phase voltage amplitude and phase angle at each f_d using discrete Fourier transformation based on the parameters in Table III and Table IV [5], [22]. Correspondingly, a fourth-order linear transfer function approximation of the measured DF is derived using the '*tfest*' function available in MATLAB, i.e.,

$$DF(s) = \frac{-1.587e17}{s^4 + 1.79e4s^3 + 3.83e7s^2 - 4.3e13s - 1.51e17}. \tag{19}$$

Meanwhile, the closed-loop transfer function from reference voltage to output voltage using conventional cascaded linear control in Fig. 3 is calculated as

$$G_l(s) = \frac{\left(k_{pv}s^2 + k_{rv}s + k_{pv}\omega_n^2\right) k_{pi}}{sC_f\left(sL_f + k_{pi} + k_{pv}k_{pi}\right)\left(s^2 + \omega_n^2\right) + k_{rv}k_{pi}s}. \tag{20}$$

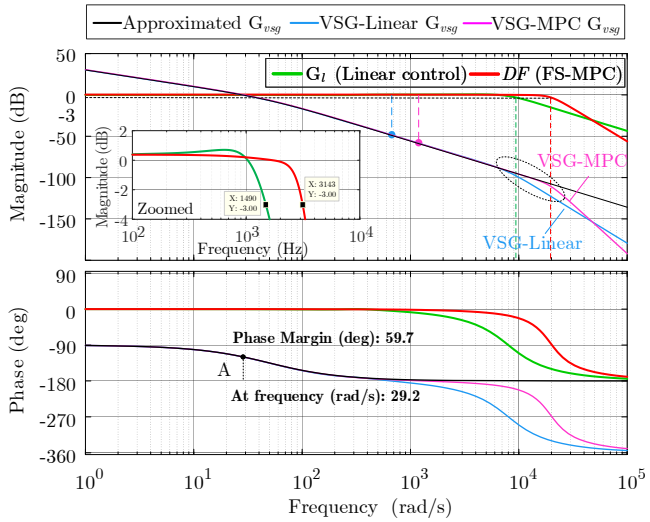

Fig. 8. Comparison of bode plot of conventional VSG-Linear control and proposed VSG-MPC.

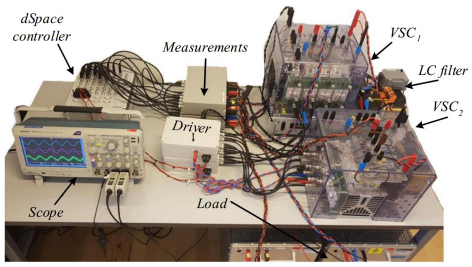

Fig. 9. Experimental platform for validating the proposed VSG-MPC.

Consequently, the transfer function of overall VSG with two inner-loop methods above is derived based on [21] as

$$G_{vsg}(s) = G_P(s)G_{vsc}(s)H_{Line0}(s) \tag{21}$$

where the transfer function from active power to electric potential angle: $G_P(s) = \frac{1}{J\omega_n s + D'}\frac{1}{s}$, $G_{vsc}(s) = DF(s)$ or $G_l(s)$, and $H_{Line0}(s) = \frac{3}{2}\frac{V_n X}{R^2+X^2}$ with $R = R_{line} + R_v$, and the transfer function for the output power to the electric potential phase angle in the low-frequency range: $X = \omega_n(L_{line} + L_v)$ in the low frequency range. Then, the bode plots of the proposed FS-MPC $DF(s)$ (red line), cascaded linear control $G_l(s)$ (green line), approximated $G_{vsg}(s)$ (with $G_{vsc}(s) = 1$, black line), VSG-Linear $G_{vsg}(s)$ (with linear control $G_{vsc}(s) = G_l(s)$, blue line), VSG-MPC $G_{vsg}(s)$ (with FS-MPC $G_{vsc}(s) = DF(s)$, pink line) are compared in Fig. 8. As is shown, for inner-loop control, the proposed FS-MPC results in a larger bandwidth than linear control, improving the voltage dynamic response. Besides, the crossover frequency ω_{co} of all three $G_{vsg}(s)$ (overlapped point A) is 29.2 rad/s with a 59.7° phase margin. Hence, the overall VSG is stable ($\omega_{co} < D'/(J\omega_n) = 50$ rad/s, and $\omega_{co} < 0.1\omega_n$ = 31.4 rad/s [21]). Moreover, the proposed VSG-MPC has a larger magnitude margin than that of conventional VSG-Linear control, enhancing system stability and robustness.

TABLE III
SYSTEM PARAMETERS OF A TWO-VSC BASED AC MG

Description	Symbol and value
Nominal voltage and frequency	V_n = 200 V, f_n = 50 Hz
DC bus voltage	V_{dc} = 500 V
Output LC filter	L_f = 2.4 mH, C_f = 15 μF
Sampling time and dead time	T_s = 25 μs, T_d = 4 μs
Line impedance	$R_{line} = 0.1\ \Omega$, $L_{line} = 1.8$mH
Cut-off frequency of low-pass filter	ω_c = 100 Hz
Average switching frequency	$f_{asw} \approx 8$ kHz
Nominal active and reactive power	$P_n = Q_n = 0$ kW
Load and virtual impedance	$R_L = 30\ \Omega$, $R_v = 1\ \Omega$, $L_v = 0.01$H
Nonlinear diode-bridge-rectifier load	R = 465 Ω, L = 1.8 mH, C = 2.2 mF

TABLE IV
CONTROLLER PARAMETERS

Controller	Symbol and value	Controller	Symbol and value
VSG & Droop	$k_p = 2\times10^{-3}$	Cascaded linear control	$k_{pv} = 0.1$
	$k_q = 5\times10^{-3}$		$k_{rv} = 30$
	$D' = D + k_\omega = 500$		$k_{pi} = 24$
	$J = 0.032$ kg·m^2	Proposed FS-MPC	$\lambda = 3$

V. SIMULATION AND EXPERIMENTAL RESULTS

A. Testbed and Configuration Description

The proposed VSG-MPC scheme is verified on a laboratory prototype as shown in Fig. 9, which consists of 18-kW-rated inverters, LC filters, DC power supplies, linear and nonlinear loads. All control algorithms are executed in a dSPACE DS1202 PowerPC DualCore 2-GHz processor board with the parameters listed in Table III and IV, where P_n and Q_n are set as 0 kW to autonomously form an islanded ac MG. Comparative simulations in MATLAB/Simulink and experiments with conventional Droop-Linear control, VSG-Linear control, and Droop-MPC are implemented to validate the effectiveness of the proposed VSG-MPC. For the proposed inner-loop FS-MPC scheme, the weighting factor is set as $\lambda = 3$ using an artificial-neural-network strategy with a heuristic 'branch and bound' method [22]. For conventional inner-loop linear control, the current-loop gain is set as $K_{pi} = 24$ (resulting in a bandwidth $f_{bw} \approx 1.6$ kHz), while the voltage-loop PR control gains are $K_{pv} = 0.1$ (resulting in a bandwidth ≈ 150 Hz) and $K_{rv} = 30$ [5]. For a fair comparison, the droop coefficient, virtual inertia, and cut-off frequency of the low-pass filter in (14) and (16) are the same for all control methods.

Considering that the proposed FS-MPC scheme has a variable switching frequency, its sampling period is set as T_s = 25 μs, which can obtain an effective switching frequency of about 7.8 kHz. For a fair comparison, the sampling period of conventional linear-control based schemes is set as 62.5 μs to obtain a similar switching frequency of 8 kHz [23]. In addition, the turnaround time measured for the proposed VSG-MPC is 17 μs, which is smaller than that of VSG-Linear control, 22 μs. Hence, the computational burden is reduced.

B. Evaluation of Static and Dynamic Performance

1) Local Voltage Response: To evaluate the steady-state and dynamic performance of the local voltage, Fig. 10 and

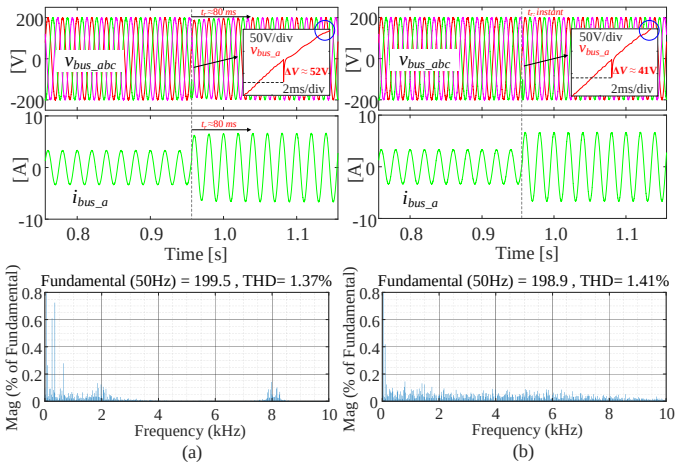

Fig. 10. Simulation results of local voltage response under a load step change and its harmonic spectrum. (a) Conventional VSG-Linear control. (b) Proposed VSG-MPC.

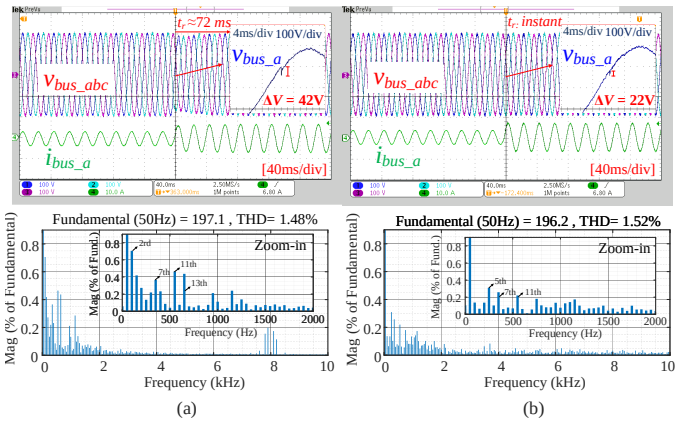

Fig. 11. Experimental results of local voltage response under a load step change and its harmonic spectrum. (a) Conventional VSG-Linear control. (b) Proposed VSG-MPC.

Fig. 11 show the simulation and experimental results of local voltage and current response under a load step change using conventional VSG-Linear control and proposed VSG-MPC, respectively. As is shown, simulation results conform well with the experimental results. In load-step transient process, both voltage fluctuation and settling time using conventional VSG-Linear control are much larger than using proposed VSG-MPC. Moreover, the proposed VSG-MPC achieves an instantaneous voltage restoration capability. In the steady state, as indicated by the zoom-in voltage and harmonic spectra, harmonics using VSG-Linear control concentrate in the odd harmonics within 2 kHz and the switching frequency harmonics, around 8 kHz. In contrast, the proposed method has a spread harmonic spectrum distributed over a wide range of frequency since the inner-loop FS-MPC does not use a modulator [7]. Nevertheless, the introduction of the dual-objective CF in (8) assures the proposed VSG-MPC to operate with a comparable steady-state performance (a little bit larger THD but acceptable) as conventional VSG-Linear control. In summary, faster dynamic response, stronger robustness to load disturbances, and desired steady-state performance of local

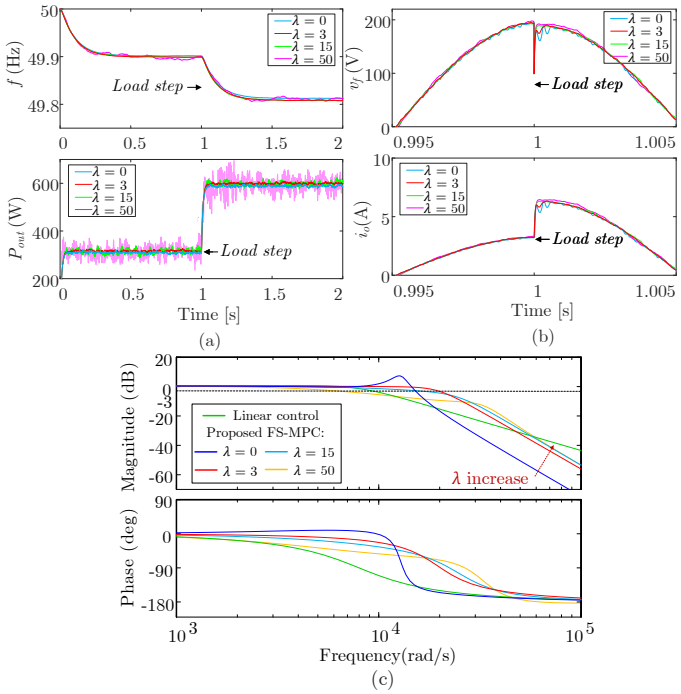

Fig. 12. Simulation comparison of proposed VSG-MPC under a load step change with different weighting factor λ. (a) Frequency and active power response. (b) Local voltage and current response. (c) DF of the proposed FS-MPC.

voltage can be obtained by the proposed method.

2) Influence of the Weighting Factor: Note that different weighting factor λ may affect the system performance. Fig. 12 depicts the simulation comparison of steady-state and dynamic response of local voltage, frequency, and active power with a varying λ, where the DF of proposed FS-MPC is also depicted. As is shown, in the case of $\lambda = 0$, the proposed FS-MPC is degraded into conventional single-objective FS-MPC, which leads to a significant steady-state voltage tracking error and a resonance peak (under-damped, inducing an overshoot, see the lower P_{out} in Fig. 12 (a) and the blue line in Fig. 12 (c)), and a large settling time under a load step change. In the case of $\lambda > 0$ (within an appropriate range), both steady-state and dynamic performance are enhanced. A larger λ can improve the transient response (see $\lambda = 3$ and 15), i.e., lower voltage settling time, while a too-large λ may deteriorate the steady-state performance and bandwidth (see $\lambda = 50$, over-damped). Hence, a tradeoff should be made to balance the static and dynamic performance in the selection of λ. It should be mentioned that the proposed VSG-MPC can easily guarantee better performance than VSG-Linear control over a large range of λ.

3) System Frequency and Active Power Sharing: Fig. 13 and Fig. 14 present the simulation and experimental results of system frequency response and active power sharing under a load step change using conventional Droop-Linear, VSG-Linear, Droop-MPC, and VSG-MPC schemes. It can be seen that typical droop-based control schemes have larger ROCOF than that of VSG-based control schemes. In other words, VSG-based control schemes can increase the system inertia.

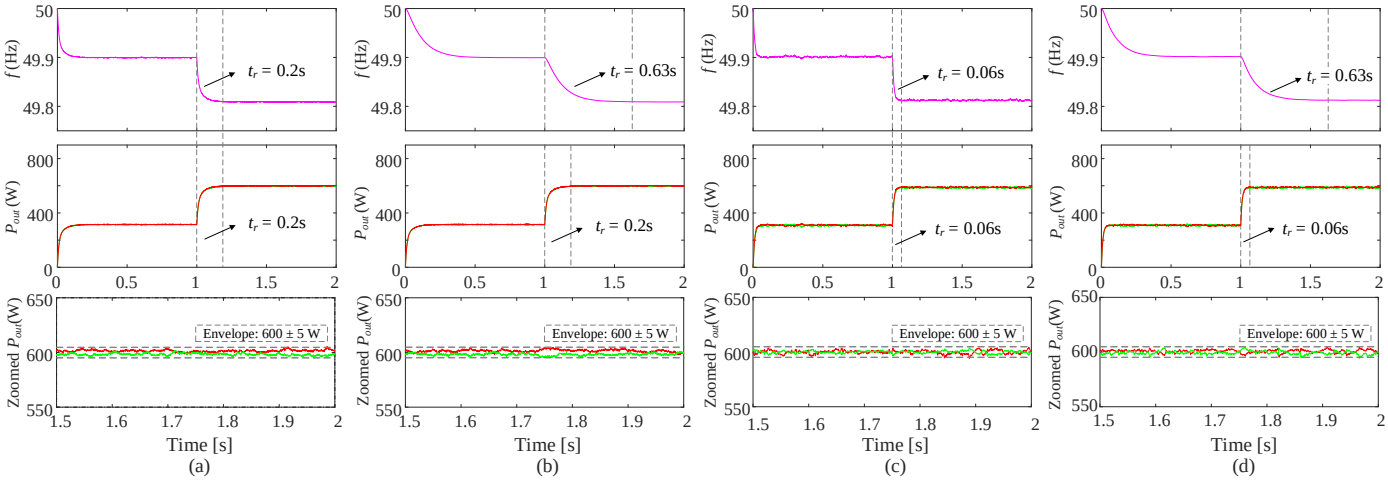

Fig. 13. Simulation results of system frequency and active power sharing under a load-step change. (a) Droop-Linear control. (b) VSG-Linear control. (c) Droop-MPC. (d) Proposed VSG-MPC.

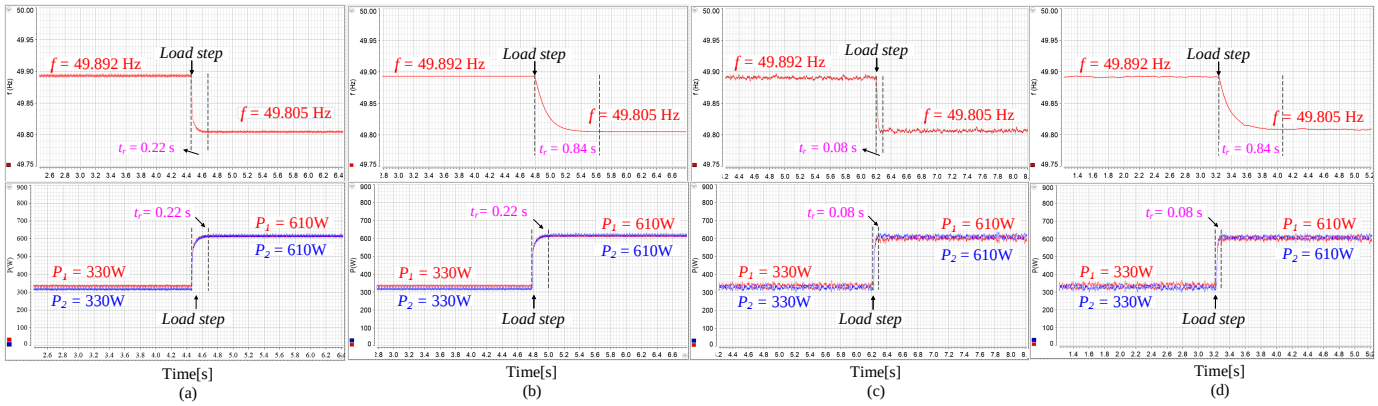

Fig. 14. Experimental results of system frequency and active power sharing under a load-step change [Obtained from dSPACE ControlDesk]. (a) Droop-Linear control. (b) VSG-Linear control. (c) Droop-MPC. (d) Proposed VSG-MPC.

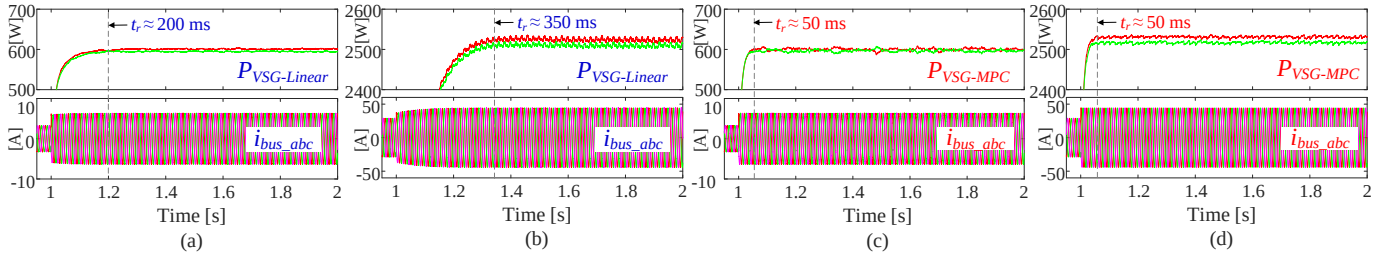

Fig. 15. Simulation results of active power ripple under different power levels. (a) Conventional VSG-Linear control at 0.6 kW. (b) Conventional VSG-Linear control at 2.5 kW. (c) Proposed VSG-MPC at about 0.6 kW. (d) Proposed VSG-MPC at about 2.5 kW.

Besides, under the output power level below 1 kW, MPC-based control schemes show a little bit larger active-power ripple than conventional linear-control based schemes, which is somewhat worse in experiments than in simulations. The reason could be that the dead time (4 μs) of 18-kW-rated VSCs has a more significant effect on the steady-state performance of the modulator-less FS-MPC at low output-power levels. This effect can be alleviated with the increase of the output power, and a comprehensive evaluation of the active-power ripple will be elaborated in the next subsection. Nevertheless, it is important to notice that a much faster active-power dynamic response is achieved using the proposed VSG-MPC compared to conventional Droop-Linear or VSG-Linear control, which is consistent with the results in Fig. 11.

C. Evaluation of Active Power Ripple

Theoretically, the active power ripple is determined by the output voltage and current of each VSC. Compared with the conventional VSG-Linear control, the active-power ripple of the proposed VSG-MPC is determined by the quantization error of converter voltage vector, which is bounded and relatively stable under different load power levels [24]. To intuitively evaluate the active-power ripple, Fig. 15 depicts the simulated active-power sharing response at different load power levels

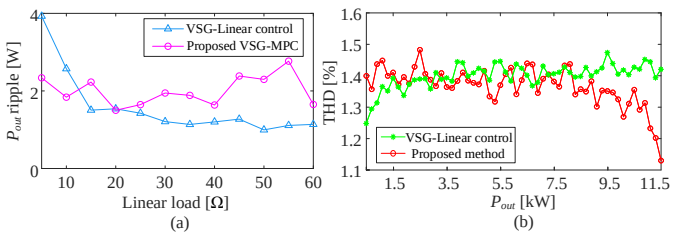

Fig. 16. Simulation evaluation of steady-state active-power ripple and voltage THD using VSG-Linear control and proposed VSG-MPC under different loads. (a) Active power ripple. (b) Voltage THD.

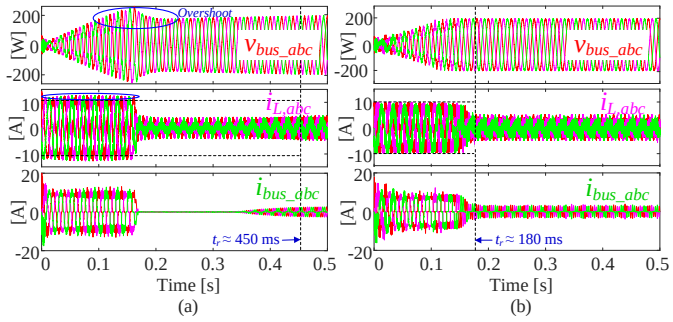

Fig. 17. Simulation results of current-limiting capability in system starting-up process under a nominal nonlinear load. (a) Conventional VSG-Linear control. (b) Proposed VSG-MPC.

using conventional VSG-Linear control and proposed method. As is shown, when the load power is about 600 W, the ripple magnitude with proposed method is slightly larger than VSG-Linear control. Nonetheless, when the load power increases by about 2.5 kW, the active-power ripple of the proposed method is reduced without sacrificing the dynamic performance (t_r maintains 50 ms), while the power ripple of VSG-Linear control is increased and the settling time is also longer (t_r increases from 200 ms to 350 ms). This mainly owns to the stronger robustness and higher-bandwidth of the proposed FS-MPC, which assures a faster transient response and enhanced load adaptability. Moreover, Fig. 16 illustrates the quantitative simulation evaluation of steady-state active-power ripple (root-mean-square) and voltage THD using VSG-Linear control and proposed VSG-MPC under different linear loads, where the active power ripple is calculated by

$$P_{out,rip} = \sqrt{\frac{1}{N}\sum_{i=1}^{N}\left(P_{out} - P_{out,avg}\right)^2} \tag{22}$$

where $P_{out,rip}$ is the calculated active power ripple, P_{out} is instant active power, $P_{out,avg}$ is average active power, and N is the sampling point number.

As is shown in Fig. 16, under the light-load condition, conventional VSG-Linear control has a lower active-power ripple and voltage THD than proposed VSG-MPC. Nonetheless, with the increase of the load power, both active-power ripple and voltage THD with conventional VSG-Linear control show a slight increase and tend to exceed the proposed method. Fortunately, the active-power ripple and its variations of both methods are small compared to the average value of the active power and are thus negligible.

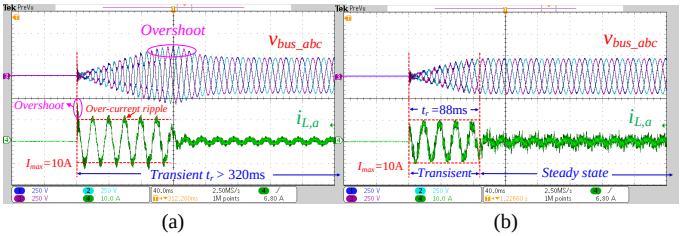

Fig. 18. Experimental results of current-limiting capability in system starting-up process under a nominal nonlinear load. (a) Conventional VSG-Linear control. (b) Proposed VSG-MPC.

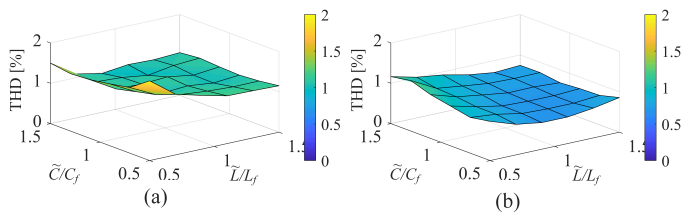

Fig. 19. Simulation evaluation of sensitivity of output voltage to model mismatches. (a) Conventional VSG-Linear control. (b) Proposed VSG-MPC.

Besides, some effective solutions are provided to further reduce the active power ripple of proposed VSG-MPC. One is to increase the sampling frequency (i.e., to decrease the sampling period) (e.g., from $T_s = 25$ μs in this paper to $T_s = 20$ μs) [23], and the other is to include a digital filter in the CF to shape the harmonics spectrum of the local voltage [25]. It is vital to notice that these solutions are the inherent merits of FS-MPC compared with conventional linear control, i.e., flexible switching frequency regulation and inclusion of multiple control objectives.

D. Evaluation of Current-Limiting Capability

To validate that the proposed VSG-MPC has an enhanced current-limiting capability over conventional VSG-Linear control for over-current protection, simulation and experimental results of current-limiting capability in system starting-up process under a nonlinear load are depicted in Fig. 17 and Fig. 18 with the maximum inductor current limit $I_{max} = 10$ A. The realization of the current-limiting using proposed method is based on (11), while conventional VSG-Linear control employs a phasor-diagram based scheme (using *Eqs.*(26) and (27) in [26]), i.e., based on (6) in this paper

$$\bar{v}_{\text{lim,ref}} = \begin{cases} \bar{v}_{\text{ref}} & ,|\bar{i}^{p}_{f,k+2}| \leq I_{\max} \\ \dfrac{\bar{i}^{p}_{f,k+2}}{|\bar{i}^{p}_{f,k+2}|} I_{\max} - \gamma & ,|\bar{i}^{p}_{f,k+2}| > I_{\max} \end{cases} \tag{23}$$

where $\gamma = \Phi_{11}\bar{i}^{p}_{f,k+1} + \Phi_{12}\bar{v}^{p}_{f,k+1} + \Gamma_{12}\bar{i}_{o,k+1}$, $\bar{v}_{\text{ref}}$ is the original converter output voltage reference for PWM modulation, while $\bar{v}_{\text{lim,ref}}$ is the modified converter voltage reference with current limitation.

It can be seen from Figs. 17 and 18 that the simulation results conform well with the experimental results. The transient rising time using conventional VSG-Linear control is much longer ($t_r > 300$ ms) than that of proposed VSG-MPC ($t_r < 200$ ms). Besides, large output voltage and inductor current

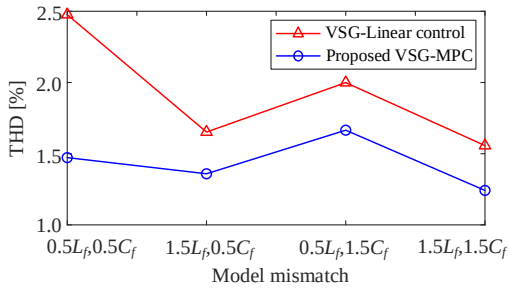

Fig. 20. Experimental evaluation of sensitivity of output voltage to model mismatches. (a) Conventional VSG-Linear control. (b) Proposed VSG-MPC.

overshoots are induced in VSG-Linear control, which would cause adverse shocks to ac MGs. Moreover, it is important to notice that the inductor-current ripple unavoidably exceeds the maximum current limit of $I_{max} = 10$ A since VSG-Linear control employs the state-space-averaging based strategy in (23). Consequently, the strict current limitation cannot be guaranteed by conventional VSG-Linear control.

In stark contrast, the proposed VSG-MPC has faster voltage stabilization with no overshoot. The inductor current is strictly limited within the preset $I_{max} = 10$ A without an over-current ripple. The reason is that the current-limiting principle of the proposed VSG-MPC is different from that of VSG-Linear control. Once the future inductor current tends to exceed the preset I_{max} in (11), corresponding candidate voltage vectors in Fig. 5 will be directly discarded from the CF evaluation. As a result, strict current-limiting capability can be assured by the proposed method, which also facilitates the smooth transition between islanded mode and grid-connected mode, enhancing the plug-and-play capability.

E. Sensitivity to Model Mismatches

Fig. 19 and Fig. 20 depict the quantitative simulation and experimental comparison of the sensitivity of output voltage to model mismatches (i.e., changing $\pm 50\%$ of nominal C_f and L_f in the controller) using conventional VSG-Linear control and proposed VSG-MPC. As is shown in Fig. 19, the proposed VSG-MPC has a lower output-voltage THD than that of conventional VSG-Linear control under a wide range of parameter variations in filter inductance and capacitance. The same conclusion can be drawn from the experimental evaluation (we choose four typical cases) in Fig. 20 that the steady-state voltage THD using both methods show a similar trend under the same model mismatches. Nonetheless, the proposed VSG-MPC still has a lower output-voltage THD, which indicates it is less sensitive (i.e., stronger robustness) to model mismatches compared with conventional VSG-Linear control.

VI. Conclusion

This paper proposes a VSG-MPC scheme for islanded ac MGs to optimize conventional primary control. First, to tackle the complex parameter-tuning effort and limited dynamic response of conventional dual-loop linear control, an improved inner-loop FS-MPC is proposed, which obtains faster and robust voltage-transient responses and strict current-limiting capability. Then, a simplified VSG is deployed in the outer control loop, achieving an accurate active power-sharing and inertia emulation. The combination of an improved FS-MPC with a simplified VSG gives full play to the superiority of both approaches and enhances the system stability, which is proved by the frequency-domain bode plot analysis. Simulation and experimental results verify the applicability of the proposed control scheme.

References

[1] J. Rocabert, A. Luna, F. Blaabjerg, and P. Rodríguez, "Control of power converters in ac microgrids," *IEEE Trans. Power Electron.*, vol. 27, no. 11, pp. 4734–4749, Nov. 2012.

[2] T. Dragicevic, "Dynamic stabilization of DC microgrids with predictive control of point-of-load converters," *IEEE Trans. Power Electron.*, vol. 33, no. 12, pp. 10 872–10 884, Dec. 2018.

[3] A. Bidram and A. Davoudi, "Hierarchical structure of microgrids control system," *IEEE Trans. Smart Grid*, vol. 3, no. 4, pp. 1963–1976, Dec. 2012.

[4] M. Shahparasti, M. Mohamadian, A. Yazdian, A. A. Ahmad, and M. Amini, "Derivation of a stationary-frame single-loop controller for three-phase standalone inverter supplying nonlinear loads," *IEEE Trans. Power Electron.*, vol. 29, no. 9, pp. 5063–5071, Sep. 2013.

[5] X. Quan, X. Dou, Z. Wu, M. Hu, H. Song, and A. Q. Huang, "A novel dominant dynamic elimination control for voltage-controlled inverter," *IEEE Trans. Ind. Electron.*, vol. 65, no. 8, pp. 6800–6812, Aug. 2018.

[6] T. Dragicevic, "Model predictive control of power converters for robust and fast operation of ac microgrids," *IEEE Trans. Power Electron.*, vol. 33, no. 7, pp. 6304–6317, Jul. 2018.

[7] S. Vazquez, J. Rodriguez, M. Rivera, L. G. Franquelo, and M. Norambuena, "Model predictive control for power converters and drives: advances and trends," *IEEE Trans. Ind. Electron.*, vol. 64, no. 2, pp. 935–947, Feb. 2017.

[8] C. Zheng, T. Dragicevic, and F. Blaabjerg, "Current-sensorless finite-set model predictive control for LC-filtered voltage source inverters," *IEEE Trans. Power Electron.*, vol. 35, no. 1, pp. 1086–1095, Jan. 2020.

[9] J. Jongudomkarn, J. Liu, and T. Ise, "Virtual synchronous generator control with reliable fault ride-through ability: A solution based on finite-set model predictive control," *IEEE J. Emerg. Sel. Top. Power Electron.*, pp. 1–1, 2019.

[10] S. D'Arco and J. A. Suul, "Equivalence of virtual synchronous machines and frequency-droops for converter-based microgrids," *IEEE Trans. Smart Grid*, vol. 5, no. 1, pp. 394–395, Jan. 2014.

[11] J. Liu, Y. Miura, and T. Ise, "Comparison of dynamic characteristics between virtual synchronous generator and droop control in inverter-based distributed generators," *IEEE Trans. Power Electron.*, vol. 31, no. 5, pp. 3600–3611, May. 2016.

[12] H.-P. Beck and R. Hesse, "Virtual synchronous machine," in *2007 9th Int. Conf. Electr. Power Qual. Util.* IEEE, Oct. 2007, pp. 1–6.

[13] P. Rodriguez, C. Citro, J. I. Candela, J. Rocabert, and A. Luna, "Flexible grid connection and islanding of SPC-based PV power converters," *IEEE Trans. Ind. Appl.*, vol. 54, no. 3, pp. 2690–2702, May. 2018.

[14] Q. C. Zhong and G. Weiss, "Synchronverters: inverters that mimic synchronous generators," *IEEE Trans. Ind. Electron.*, vol. 58, no. 4, pp. 1259–1267, Apr. 2011.

[15] J. Chen, M. Liu, and T. O'Donnell, "Replacement of synchronous generator by virtual synchronous generator in the conventional power system," in *2019 IEEE Power Energy Soc. Gen. Meet.* IEEE, Aug. 2019, pp. 1–5.

[16] X. Meng, J. Liu, and Z. Liu, "A generalized droop control for grid-supporting inverter based on comparison between traditional droop control and virtual synchronous generator control," *IEEE Trans. Power Electron.*, vol. 34, no. 6, pp. 5416–5438, Jun. 2019.

[17] S. D'Arco, J. A. Suul, and O. B. Fosso, "Automatic tuning of cascaded controllers for power converters using eigenvalue parametric sensitivities," *IEEE Trans. Ind. Appl.*, vol. 51, no. 2, pp. 1743–1753, Mar. 2015.

[18] F. de Bosio, L. A. Ribeiro, F. D. Freijedo, M. Pastorelli, and J. M. Guerrero, "Effect of state feedback coupling and system delays on the transient performance of stand-alone VSI with LC output filter," *IEEE Trans. Ind. Electron.*, vol. 63, no. 8, pp. 4909–4918, 2016.

[19] P. Cortés, G. Ortiz, J. I. Yuz, J. Rodríguez, S. Vazquez, and L. G. Franquelo, "Model predictive control of an inverter with output LC filter for UPS applications," *IEEE Trans. Ind. Electron.*, vol. 56, no. 6, pp. 1875–1883, Jun. 2009.
[20] M. Guan, W. Pan, J. Zhang, Q. Hao, J. Cheng, and X. Zheng, "Synchronous generator emulation control strategy for voltage source converter (vsc) stations," *IEEE Trans. Power Syst.*, vol. 30, no. 6, pp. 3093–3101, Nov. 2015.
[21] J. Chen and T. O'Donnell, "Parameter constraints for virtual synchronous generator considering stability," *IEEE Trans. Power Syst.*, vol. 34, no. 3, pp. 2479–2481, May. 2019.
[22] T. Dragičević and M. Novak, "Weighting factor design in model predictive control of power electronic converters: An artificial neural network approach," *IEEE Trans. Ind. Electron.*, vol. 66, no. 11, pp. 8870–8880, Nov. 2019.
[23] H. A. Young, M. A. Perez, J. Rodriguez, and H. Abu-Rub, "Assessing finite-control-set model predictive control: a comparison with a linear current controller in two-level voltage source inverters," *IEEE Ind. Electron. Mag.*, vol. 8, no. 1, pp. 44–52, Mar. 2014.
[24] R. P. Aguilera and D. E. Quevedo, "Predictive control of power converters: Designs with guaranteed performance," *IEEE Trans. Ind. Informatics*, vol. 11, no. 1, pp. 53–63, Feb. 2015.
[25] P. Cortés, J. Rodríguez, D. E. Quevedo, and C. Silva, "Predictive current control strategy with imposed load current spectrum," *IEEE Trans. Power Electron.*, vol. 23, no. 2, pp. 612–618, Mar. 2008.
[26] H. Kim, H. Jung, and S. Sul, "Discrete-time voltage controller for voltage source converters with lc filter based on state-space models," *IEEE Trans. Ind. Appl.*, vol. 55, no. 1, pp. 529–540, Jan. 2019.

Changming Zheng (S'19) received the B.Sc. degree in 2014 from the College of Control Science and Engineering, China University of Petroleum (East China), Qingdao, China, where he is currently working toward the Ph.D. degree in power electronics. From 2018 until 2020, he has been a Visiting Ph.D. Student with the Department of Energy Technology, Aalborg University, Aalborg, Denmark.

His research interests include model predictive control, application of advanced control in renewable energy systems, DC/AC microgrids, and permanent magnet synchronous motor drives.

Tomislav Dragičević (S'09-M'13-SM'17) received the M.Sc. and the industrial Ph.D. degrees in Electrical Engineering from the Faculty of Electrical Engineering, University of Zagreb, Croatia, in 2009 and 2013, respectively. From 2013 until 2016 he has been a Postdoctoral researcher at Aalborg University, Denmark. From 2016 until 2020 he was an Associate Professor at Aalborg University, Denmark. From 2020 he is a Professor at the Technical University of Denmark.

His research interest is application of advanced control, optimization and artificial intelligence inspired techniques to provide innovative and effective solutions to emerging challenges in design, control and cybersecurity of power electronics intensive electrical distributions systems and microgrids. He has authored and co-authored more than 200 technical publications (more than 100 of them are published in international journals, mostly in IEEE), 8 book chapters and a book in the field.

He serves as an Associate Editor in the IEEE TRANSACTIONS ON INDUSTRIAL ELECTRONICS, in IEEE TRANSACTIONS ON POWER ELECTRONICS, in IEEE Emerging and Selected Topics in Power Electronics and in IEEE Industrial Electronics Magazine. Dr. Dragičević is a recipient of the Končar prize for the best industrial PhD thesis in Croatia, a Robert Mayer Energy Conservation award, and he is a winner of an Alexander von Humboldt fellowship for experienced researchers.

Frede Blaabjerg (S'86–M'88–SM'97–F'03) was with ABB-Scandia, Randers, Denmark, from 1987 to 1988. From 1988 to 1992, he got the PhD degree in Electrical Engineering at Aalborg University in 1995. He became an Assistant Professor in 1992, an Associate Professor in 1996, and a Full Professor of power electronics and drives in 1998. From 2017 he became a Villum Investigator. He is honoris causa at University Politehnica Timisoara (UPT), Romania and Tallinn Technical University (TTU) in Estonia.

His current research interests include power electronics and its applications such as in wind turbines, PV systems, reliability, harmonics and adjustable speed drives. He has published more than 600 journal papers in the fields of power electronics and its applications. He is the co-author of four monographs and editor of ten books in power electronics and its applications.

He has received 32 IEEE Prize Paper Awards, the IEEE PELS Distinguished Service Award in 2009, the EPE-PEMC Council Award in 2010, the IEEE William E. Newell Power Electronics Award 2014, the Villum Kann Rasmussen Research Award 2014, the Global Energy Prize in 2019 and the 2020 IEEE Edison Medal. He was the Editor-in-Chief of the IEEE TRANSACTIONS ON POWER ELECTRONICS from 2006 to 2012. He has been Distinguished Lecturer for the IEEE Power Electronics Society from 2005 to 2007 and for the IEEE Industry Applications Society from 2010 to 2011 as well as 2017 to 2018. In 2019-2020 he serves a President of IEEE Power Electronics Society. He is Vice-President of the Danish Academy of Technical Sciences too. He is nominated in 2014-2019 by Thomson Reuters to be between the most 250 cited researchers in Engineering in the world.